Journal of Energy Storage 84 (2024) 110675

Contents lists available at ScienceDirect

Journal of Energy Storage

journal homepage: www.elsevier.com/locate/est

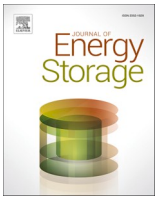

Research papers

Study of paraffinic and biobased microencapsulated PCMs with reduced graphene oxide as thermal energy storage elements in cement-based materials for building applications

E. Erkizia [a,*], C. Strunz [b], J.-L. Dauvergne [c], G. Goracci [d], I. Peralta [e,f,g], A. Serrano [c], A. Ortega [h], B. Alonso [h], F. Zanoni [i], M. Düngfelder [b], J.S. Dolado [d,k], J.J. Gaitero [a,j], C. Mankel [e], E. Koenders [e]

[a] TECNALIA, Basque Research and Technology Alliance (BRTA), Derio 48160, Spain
[b] NETZSCH Geratebau GMBH, Selb 95100, Germany
[c] Center for Cooperative Research on Alternative Energies (CIC energiGUNE), Basque Research and Technology Alliance (BRTA), 01510 Vitoria-Gasteiz, Spain
[d] Centro de Física de Materiales (CSIC-UPV/EHU) 20018 Donostia-San Sebastián, Spain
[e] Institute of Construction and Building Materials, TU Darmstadt, Germany
[f] Centro de Investigación de Métodos Computacionales (CIMEC), UNL-CONICET, Predio CONICET "Dr. Alberto Cassano", 3000 Santa Fe, Argentina
[g] Laboratorio de Flujometría (FLOW), FRSF-UTN, Lavaise 610, 3000 Santa Fe, Argentina
[h] GRAPHENEA, SA, San Sebastian 20009, Spain
[i] SPHERA ENCAPSULATION SRL, Dossobuono, Verona 37069, Italy
[j] Department of Physics, University of the Basque Country UPV/EHU, Barrio Sarriena s/n, 48940, Leioa, Spain
[k] Donostia International Physics Center (DIPC), Paseo Manuel de Lardizabal 4, 20018 Donostia-San Sebastián, Spain

ARTICLE INFO

Keywords:
Thermal energy storage
Microencapsulated phase change materials
Biobased PCM
Paraffinic PCM
Reduced graphene oxide
Cement-based materials

ABSTRACT

Addition of different types of phase change materials (PCMs) to cement-based materials for thermal energy storage has been broadly investigated in the literature. Many studies have researched the addition of organic PCMs and the thermal performance of the PCM-cement system. However, drawbacks such as leakage and poor thermal conductivity of the PCMs have stimulated studies to improve thermal properties within the PCM-cement system. Among the different solutions, addition of carbonous materials (such as graphite and carbon nanotubes) to improve thermal conductivity of the PCMs have been investigated. In the current work, an innovative system that contains microencapsulated PCMs (MPCMs) and purposely synthesized reduced graphene oxide (rGO) has been designed and assessed. The addition of rGO has two aims. The first one is to speed up the heat storage/release velocity by improving the thermal conductivity of the whole system. The second one is to improve the electrical conductivity of the system in order to actively (by applying voltage) be able to turn on the thermal storage/release feature. Up to the authors' knowledge, this is a novel approach for the development of active PCM-cement based thermal energy storage systems. Furthermore, in the present study, the use of paraffinic PCMs was compared with that of biobased PCMs in order to provide a more sustainable solution to the design of cement-based elements for buildings applications. A comprehensive thermal characterization (heat storage capacity, thermal conductivity and diffusivity) has been carried out as well as microstructural characterization. Moreover, broadband dielectric spectroscopy was used to characterize the electrical conductivity of the novel MPCM-rGO-cement system.

1. Introduction

Phase Change Materials (PCMs) are compounds that usually absorb or release large amounts of energy/heat at almost constant temperature when their phase transitions (solid to solid, solid to liquid, and/or liquid to gas) occur. In the field of construction materials, addition of PCMs to cement based materials has been studied, for example, to reduce early-age fracture [1–3], freeze-thaw damage [4–6] and to improve thermal comfort inside residential and tertiary buildings coupled with a reduced energy consumption [7]. PCMs can be inorganic and organic in nature, and the use of both has their advantages and drawbacks [8]. The organic PCMs show good chemical stability and high energy storage capacity,

* Corresponding author at: Parque Tecnológico de Bizkaia, Astondo Bidea, Edificio 700, 48160 Derio, Bizkaia, (Spain).
E-mail address: edurne.erkizia@tecnalia.com (E. Erkizia).

https://doi.org/10.1016/j.est.2024.110675
Received 24 October 2023; Received in revised form 11 January 2024; Accepted 28 January 2024
Available online 15 February 2024
2352-152X/© 2024 The Authors. Published by Elsevier Ltd. This is an open access article under the CC BY license (http://creativecommons.org/licenses/by/4.0/).

they are non-corrosive, they do not undergo supercooling, and they have good nucleation rate. As drawbacks, they cannot be used at high temperatures (>150 °C) and they have low density [59]. On the other hand, inorganic PCMs can work in a wider range of temperature (−100 °C and 1000 °C) compared to the organic ones but they are often corrosive materials and not appropriate for building applications [59].

To develop novel construction systems/elements (e.g., building envelopes) that could significantly cut back energy demands of buildings, one strategy is to take advantage of the different properties of diverse elements and materials and to integrate them altogether. For example, much work has been done in the development of gypsum interior wallboards with PCMs [9–19] adding latent heat storage capacity to the other properties shown by gypsum. Another option is the design of elements with cement-based materials and PCMs by combining the properties of both materials [20–23]. In fact, cement-based materials have a high sensible heat storage capacity which can be enhanced by taking advantage of the latent heat storage capacity of the PCM material. Furthermore, by playing with the amount of water to binder ratios and additives, different density porous foam-concrete could be designed, adding insulating properties to the element panel besides the energy storage capacity. Combining these properties can help to improve the thermal comfort and reduce energy expenditure, improving sustainability in the long term.

A lot of research has been carried out on organic PCMs, especially with oil derived paraffinic compounds [7 and references within]. Besides the characteristics mentioned above, one of the downsides of these paraffinic compounds, in terms of sustainability, is that they are obtained from oil refinery and moreover, they are flammable. An appealing alternative to these products is the use of bio-based compounds that show large latent-heat properties as the paraffinic ones [24]. These biobased PCMs are more sustainable and less flammable than the paraffinic ones. Nevertheless, both, biobased PCMs and paraffins, are difficult to integrate in building materials due to their poor interaction and bad dispersion in mineral composites. Furthermore, both types of PCMs also show low thermal conductivity [26,27,47], which in addition to the low thermal conductivity of the cement-based materials can further reduce the velocity at which heat can be stored and/or released during the phase change. All these limitations and their cost have prevented their widespread use in the building sector [59]. Regarding the low thermal conductivity, and in order to enhance it, different research groups have used carbon-based materials [28], such as carbon nanotubes [29] and expanded graphite as additions in the cement-based mixes [30]. Among the carbon-based nanoparticles, graphene shows extraordinary physical properties such as high electrical conductivity (~10^6 S/m) [31], high surface area (>2000 m^2/g) [32], high elastic modulus (~1.0 TPa) [33], and high thermal conductivities (~103 W/mK) [34]. In the literature, different studies can be found where authors investigate the improvement of thermal properties of the PCM with graphene addition [28 and references within]. In these studies, only the PCM-graphene system was studied, and researchers have observed an improvement in thermal conductivity when the graphene was added [28,60,61]. In this regard, the authors of the current work wanted to take advantage of the excellent thermal and electrical conductivity characteristics of graphene in order to design and prepare a PCM and a cement system with not only improved thermal conductivity but also improved electrical conductivity with the aim of producing a system whose thermal storage/release feature can be actively turned on. However, graphene is hydrophobic, and it is not very compatible with water and inorganic compounds [35]. To introduce graphene-like particles in hydrophilic materials such as cement paste, one strategy is to firstly oxidize it, and then to partially reduce it in order to recover the good thermal and electrical conductivity properties while maintaining hydrophilicity. In the current study, reduced graphene oxide (rGO) particles have been purposely synthesized to facilitate their dispersion and added to the cement systems with the aim of improving the heat storage/release velocity. Furthermore, the addition of rGO could also provide thermoelectrical coupling to the paste, i.e., the temperature of the composite could be raised by applying small voltages to the sample. This feature would allow turning on the thermal storage/release feature by actively melting or freezing the PCM.

Table 1
Available thermophysical properties of the PCMs used in this work given by the suppliers [36–38].

Phase change material (PCM)	RT24	Nextek 24D	PureTemp25
Peak melting temperature (°C)	24	24	24
Heat storage capacity (J/g)	160	≥170	≥187
Thermal conductivity (liquid) (W/(mK))	0.2	–	0.15
Thermal conductivity (solid) (W/(mK))	0.2	–	0.25
Specific heat capacity (liquid) (kJ/(kg*K))	2	–	2.2
Specific heat capacity (solid) (kJ/(kg*K))		–	1.99
Density (liquid) (kg/L)	0.88	–	0.86
Density (solid) (kg/L)	0.77	–	0.95
Thermal cycle stability	–	–	It is stable through 10,000 thermal cycles (~27.4 years of continuous daily usage)

In a previous work [53], the authors have studied the effect of the addition of different percentages of one type of paraffinic microencapsulated PCM (MPCM) combined with reduced graphene oxide in the thermal storage properties of cement-based composite. As a continuation of that study, the current work was aimed to study the behavior of a bio-PCM embedded in cement-based materials and to compare it to the more traditional and less sustainable paraffinic PCMs. In this sense, cement-based materials with a bio-based MPCM (PureTemp25, 20 % Vol.) have been prepared, characterized, and compared to cement pastes with two paraffin-based MPCMs (RT24 and Nextek 24D, 20 % Vol.). Additionally, novel MPCM-rGO-cement systems have been produced with the above mentioned phase change materials, and a comprehensive thermal characterization (phase change temperature, latent heat of fusion, thermal conductivity and diffusivity) of the cement composites has been carried out to understand the effect of these MPCMs in the thermal properties of the composites. Furthermore, the electrical conductivity of the MPCM-rGO-cement systems has also been studied by using broadband dielectric spectroscopy. Finally, morphological characterization by using scanning electron microscopy (SEM) and mercury intrusion porosimetry (MIP) was also performed to study the effect of the MPCMs in the microstructure of the cement matrix.

2. Materials and methods

2.1. Materials

Ordinary Portland cement (CEM I 52.5R) was provided by Cementos Lemona. The metakaolin (Centrilit NCII, an amorphous aluminosilicate) was obtained from MC-Bauchemie. The admixtures Centrament Rapid 500 (accelerator), Centrament Stabi 520 (stabilizer, water retainer) and MC-Powerflow 3195 superplasticizer were also provided by MC-Bauchemie. The phase change materials used were two paraffins and one bio-based compound. The paraffins were RT24, purchased from Rubitherm GmbH, and Nextek 24D (Nx24), obtained from Microtek laboratories. The biobased PCM was PureTemp25 (PT25) acquired from PureTemp LLC. Nextek 24D product is already a microencapsulated PCM whereas RT24 and PT25 were purchased as raw PCMs. Table 1 summarizes the main thermophysical properties of the PCMs according to the suppliers.

The raw RT24 and PT25 PCMs were encapsulated by Follmann GmbH & Co. KG for the current study. The microcapsules (MRT24 and

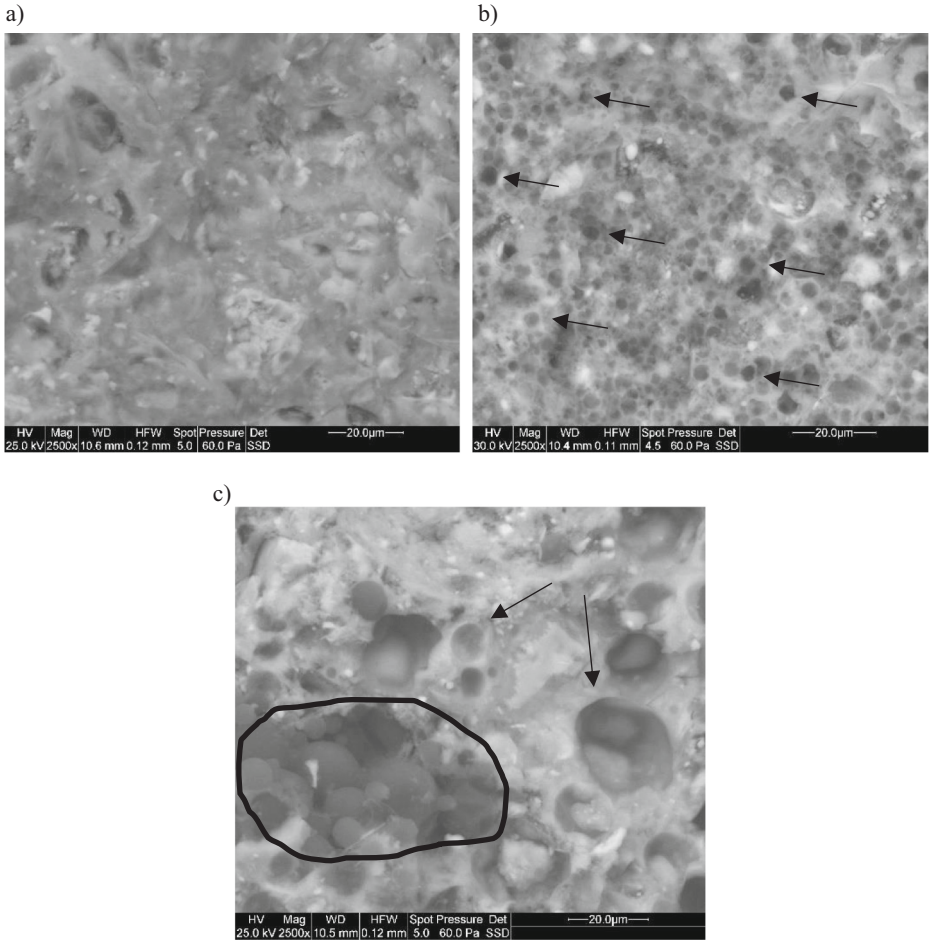

Fig. 1. SEM images of reference paste (REF-1) (a), paste with 20 % MRT24 (P1-MRT24), the arrows point to microencapsulated MRT24 (b); paste with 20 % Nx24 (P1-Nx24), the circle shows agglomerated microcapsules (Nx24) and the arrows some pores (c).

MPT25) were in a form of a powder and based on the technology SmartCaps, commercialized under the name Folco SmartCaps®. The SmartCaps technology is proprietary of Follmann GmbH & Co. KG (https://smartcaps.follmann.com/en/home-english/). The shell is organic and composed from melamine-formaldehyde (MF) obtained through polymerization technique. After the polymerization the solution is spray-dried to obtain the product in dry form. In the case of MRT24, the diameter d_{90} of the microcapsules is 12 μm and for MPT25 the size distribution is between 3 μm and 11 μm (information given by Follmann). These sizes were confirmed in the current study by the images obtained by SEM (see supplementary material fig. S3). The Nextek 24D (Nx24) was purchased already microencapsulated. In the latter case the shell is based on melamine-formaldehyde crosslinked with a crosslinking agent which contains cyclic urea and a multifunctional aldehyde

Table 2
Composition of the pastes. In the following the MRT24 and Nx24 series are denoted as P1-MRT24 and P1-Nx24, respectively. When rGO is added, the samples are denoted as P1-MRT24-rGO and P1-Nx24-rGO, respectively, and P1-rGO when the paste contains only rGO. The corresponding reference pastes are denoted as REF-1a and REF-1b, respectively. In the same way, MPT25-based samples are denoted as: P2-MPT25, P2-MPT25-rGO and REF-2. The REF-2 paste with just rGO is designated P2-rGO.

Components (g)	REF-1a	P1-rGO	P1-MRT24	P1-MRT24-rGO	REF-1b	P1-Nx24	P1-Nx24-rGO	REF-2	P2-rGO	P2-MPT25	P2-MPT25-rGO
Cem I 52.5R	100	100	100	100	100	100	100	100	100	100	100
Centrilit NCII (metakaolin)	16.46	16.46	16.46	16.46	16.46	16.5	16.5	16.46	16.46	16.46	16.46
water	38.43	*	38.43	*	38.43	38.45	*	38.43	*	38.43	*
MRT24			19.3	19.3							
Nx24						17.33	17.33				
MPT25										17.31	17.31
rGO** 0.3wt%bcw		38.77							38.43		38.43
Accelerator	2.33	2.33	2.33	2.33	2.3	2.33	2.33	2.33	2.33	2.33	2.33
Superplasticizer dispersion***	0.58	0.58	1.21	2.33	0.58	1	2.5	0.58	0.58	0.99	2.50
Stabilizer	3.37	3.37	3.38	3.38	3.37	3.37	3.37	3.37	3.37	3.37	3.37

* The required water (38.44 g for w/b = 0.33) was added with the rGO dispersion.
** rGO is a 0.89 wt% water dispersion.
*** 35 % superplasticizer content in weight. The water content of the superplasticizer was not used for the calculation of the w/b ratio.

and another crosslinker [54]. The synthesis method is proprietary of Microtek Laboratories, Inc. [54]. The mean size of the microcapsules is 15–30 μm (provided by the supplier) (characterization by SEM in the present study showed sizes between 5 and 40 μm, see Supplementary material Fig. S3). Although all the shells contain a melamine-formaldehyde based composition the formulation of shells of Follmann (MRT24 and MPT25) and Microtek Laboratories, Inc. (Nx24) are somewhat different and interact differently with the cement as it was observed in the SEM analysis carried out in the current study (see Fig. 1).

The reduced graphene oxide (rGO) was synthesized for the current study by Graphenea as a 0.89 wt% water dispersion. Graphene oxide (GO) was first produced via Hummers modified method [39] from graphite as a starting material. Then, the GO produced was dispersed in water and thermally reduced in a reflux system to produce rGO. The produced rGO was characterized by XRD, TGA and elemental analysis. The XRD diffractogram (see Supplementary material, Fig. S1) shows no crystalline peaks which is indicative of the formation of rGO. The TGA thermogram (see Supplementary material Fig. S2) shows a weight loss between 25 °C and 125 °C due to the loss of superficial water and another weight loss between 125 °C and 300 °C which is related to the release of CO, CO_2 and water. Lastly, the elemental analysis carried out of the rGO showed it contains 64.70 % of carbon, 1.13 % hydrogen, 32.31 % of oxygen, and 1.86 % of sulfur.

2.2. Paste and specimen preparation

Different cement pastes with 20 % in volume of MRT24, Nx24 and MPT25 were cast with a water/binder (w/b) ratio of 0.33. Furthermore, pastes containing 0.3 wt% rGO based on weight of binder (bwb) and 20 % in volume of MPCMs were also prepared. In Table 2 the composition of the different types of pastes are shown.

The general mixing procedure of the pastes with only rGO (P1-rGO) and with microencapsulated MRT24 and Nx24 with rGO (P1-MRT24-rGO and P1-Nx24-rGO, respectively) and without it (P1-MRT24 and P1-Nx24, respectively) are based on the one carried out in [53] but adjusting the superplasticizer for the different MPCMs. To produce the pastes with only the microencapsulated PCMs (P1-MRT24, P1-Nx24) and the corresponding reference (REF-1), the cement and metakaolin (Centrilit NCII) were mixed for 1 min at 300 rpm. Afterwards, water with the superplasticizer was added and the whole paste was mixed for 1 min at 750 rpm. Next the stabilizer was added, and the mixing continued for 30 s at 750 rpm, followed by the accelerator, mixing the paste for 30 more seconds at 750 rpm. For the reference specimens (REF-1) the paste was molded at this point. In the case of the pastes with the MPCMs, the microcapsules were added after the mixing of the accelerator, and the whole paste was mixed at 300 rpm for 1 more minute. In the case of the pastes that contain the rGO (P1-rGO, P1-MRT24-rGO, P1-Nx24-rGO) the mixing process is as follows. Cement and metakaolin were mixed for 1 min at 300 rpm. Then, the rGO dispersion was added and the whole paste was mixed for 1 min at 750 rpm. The addition of the rGO dispersion provided the correct quantity of water for a w/b ratio of 0.33 as well as the correct amount of rGO to obtain a 0.3 wt% in the paste. Next the stabilizer was added, and the mixing continued for 30 s at 750 rpm, followed by the accelerator, mixing the paste for 30 more seconds at 750 rpm. For the specimens with only rGO addition (P1-rGO), the paste was molded at this point. In the case of the pastes with the MPCMs, the microcapsules were added after the mixing of the accelerator, and the whole paste was mixed at 300 rpm for 1 more minute.

In the case of the paste with MPT25 with and without rGO, a larger volume of paste was prepared in order to study the scale up of the mixing procedure. The order of the addition of the different components was the same as for the pastes with microencapsulated MRT24 and Nx24, but the mixing was done in a bigger mixing machine and a lower mixing speed was used. The mixing procedure was like the previous one but with the following differences: firstly, the cement and metakaolin were mixed 1 min at 150 rpm; then, for the other steps, half of the speed of the previous procedure was used, and to compensate that, the time of each step was doubled. A reference paste was also prepared with this procedure (REF-2) and a paste with 0.3 wt% rGO (P2-rGO).

Once all the components were mixed, the pastes were molded, wrapped in a cling film, demolded after one day, wrapped again in cling film and cured for 28 days in a conditioned room under ambient conditions (21.0 °C and 48.9 % relative humidity) after which the different characterizations were carried out. In case of the samples for Differential Scanning Calorimetry (DSC), the samples were cast directly into the *Concavus*® crucibles for measurement and cured in there, to achieve best possible contact between the sample and the sensor.

Table 3
Dimensions of the different cast specimens.

Specimen dimension		Characterization
Height (mm)	Diameter (mm)	
3	5	Differential scanning calorimetry
20	40	Hot disk, mercury intrusion porosimetry, SEM
20	12	Laser flash technique (LFA)
5	15	Electrical conductivity measurements

2.3. Characterization techniques

To perform a full thermal and morphological characterization, different size and type of specimens were cast for each paste. In Table 3 the dimensions of the different specimens are shown.

Characterization of phase transition temperatures and melting enthalpies (latent heat capacity) was carried out via DSC. The employed device was a NETZSCH DSC 204 F1 Phoenix®. Measurement definition, data acquisition and evaluation are supported by the Proteus® software package. The instrument allows for measurements in a broad temperature range of −180 °C to 700 °C. NETZSCH Differential Scanning Calorimeters (DSC) meets the respective instrument and application standards [55]. Temperature and enthalpy calibration of the system were done for different heating rates, using a set of standards, involving Adamantane, Biphenyl, Indium, Tin, Bismuth, Zinc and Phenyl Salicylate, thereby covering a broad temperature range. To determine the phase transition temperatures and enthalpies, the samples were analyzed by subjecting each of them to heating and cooling cycles in the temperature range from-25 °C to 60 °C at two different heating rates, namely 5 K/min and 0.25 K/min under nitrogen atmosphere. The phase transition temperatures were considered the peak temperature of corresponding endothermic peaks, measured at the low heating rate of 0.25 K/min, whereas the enthalpies corresponding to the transition were calculated by peak integration and comparison of both heating runs, with low and high heating rate, since the low heating rates are more sensitive to signal noise of the instrument. However, to gain representative insights of the MPCM behavior, these low heating rates are necessary for phase change transition investigation. For the measurements, the procedure, including the respective heating rate tests described in RAL-GZ 896 were followed.

The thermal diffusivities of the cement pastes were measured by using the NETZSCH Laser Flash Apparatus (LFA 467 HyperFlash®). The unit is equipped with a furnace, which can operate from −100 °C to 500 °C. The front surface of the sample is heated by a Xenon flash lamp with variation of energy by voltage and pulse-length. The resulting temperature increase on the rear face is measured by using an IR-detector (InSb or MCT). The high data acquisition rate of 2 MHz allows for reliable and accurate measurements of high conductive thin materials. The patented ZoomOptics optimizes the detector's field of view to avoid distortions from edge effects. Various analysis models are integrated in the software. The data can be corrected for finite pulse and heat loss effects. The LFA 467 HyperFlash® operates in accordance with national and international standards such as ASTM E-1461 and DIN EN 821. Thermal diffusivities of cement pastes were investigated between

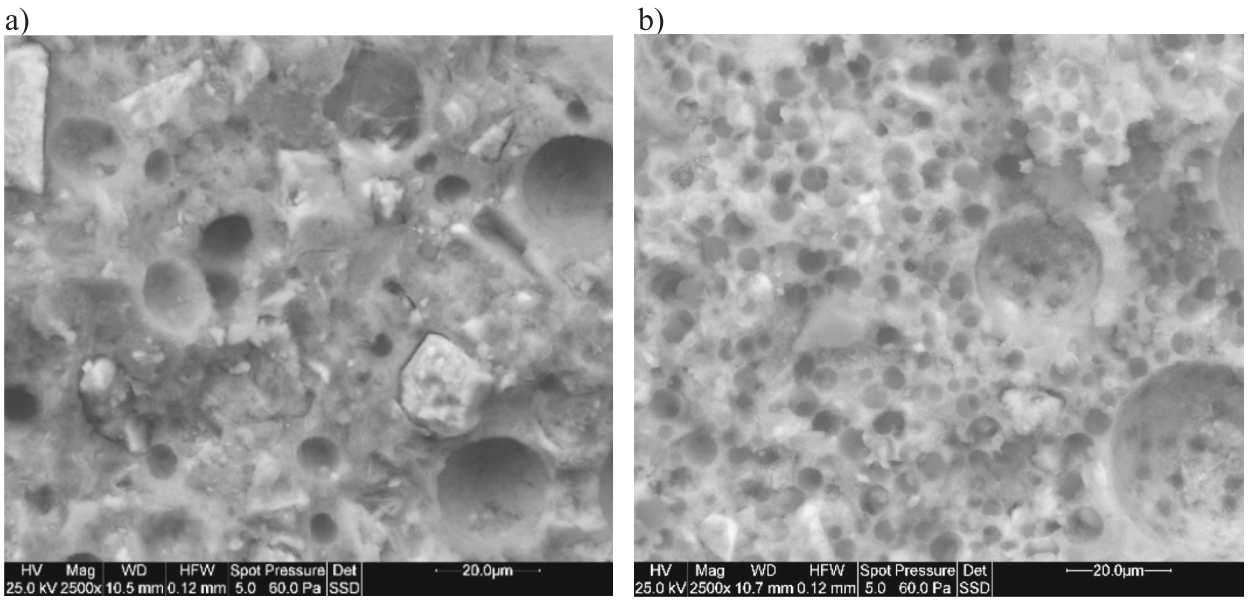

Fig. 2. (a) SEM Images of REF-2 paste. The paste shows a large porosity. (b) SEM images of P2-MPT25 paste. Besides the air pores, microparticles smaller than 10 µm can be observed well dispersed throughout the paste which are the MPT25 microcapsules.

−15 °C and 45 °C in 10 K steps in order to achieve comparable results with pastes involving MPCMs with different melting temperatures and/or melting ranges in the related temperature range.

Thermal conductivities of the cement pastes were characterized by transient plane source technique (also known as Hot Disk) [40]. Hot Disk measurements were also used to estimate thermal diffusivities and compared to the ones measured by LFA. According to measurements made on common materials from polystyrene to aluminum, the accuracy over the whole range of thermal conductivities is estimated at 2 % to 5 % for isotropic materials with a reproducibility of 2 % [41].

The size of the sensor and of the different samples, the preparation of the latter, the corresponding heating powers and measurement times were carefully chosen according to the standard Hot Disk DIN-EN-ISO 22007-2:2021–05 [42]. Thus, the thermal conductivity measurement of each cement paste was carried out on cylindrical-shaped samples (40 ± 1 mm diameter and 20 ± 1 mm thickness). A TPS 2500 S instrument equipped with a Kapton sensor of 6.403 mm in radius (sensor type 5501 F1) was employed. The power applied to the samples was 80 mW during 80 s. All the samples were tested inside a climatic chamber Binder MKFT 115 E5 (±0.1 °C with a relative humidity fixed at 60 %RH for all the experiments). The cement pastes were characterized at temperatures far enough below and above the transition temperature range of the MPCMs. Using the results of the DSC experiments (see Section 2.2), these temperatures were chosen at 5 °C (T1) and 35 °C (T2). The reference cement pastes, i.e., without incorporation of MPCMs, were also characterized at the same temperatures. At least 3 measurements were carried out for each sample by moving it between each test. The recorded data was processed using the Hot Disk Software (version 7.4.0.10).

The electrical conductivities were measured by broadband dielectric spectrometer Novocontrol Alpha-A+ in the frequency range of 10^{-1}–10^{6} Hz. MPCMs and rGO were measured in powder, sandwiched between parallel gold-plated electrodes, with a diameter of 20 mm and a sample thickness of ~0.5 mm. Prior to data acquisition, the samples were kept inside the instrument at 42 °C during 10 min to remove moisture from the sample surface. Finally, the isothermal frequency scans were performed on heating every 5 degrees over the 12–42 °C temperature range. Sample temperature was controlled with a stability better than ±0.1 K. Scanning electron microscopy images were obtained with a FEI Quanta 200 ESEM (Environmental Scanning Electron Microscope) microscope. The images were obtained by using a backscattered electron detector at 25.0 kV and 30 kV at low vacuum (60 Pa). Furthermore, this equipment includes a Fluorescence Dispersive Energy Spectrophotometer (EDAX) to analyze the elemental composition of a sample.

The porosity and pore size distribution of the different pastes were characterized by MIP. The equipment used is an Autopore III from Micromeritics Instrument Corp. MIP can detect pores between 66 nm and 360 µm. During the measurement, mercury is progressively pushed against the sample and forced to penetrate into the open porosity. As the capacity of such metal to penetrate through a hole depends not only on the pressure exerted but also on the size of the hole, the pore size distribution can be obtained applying the Washburn equation [43]. Although this methodology cannot predict with great accuracy the real pore sizes, MIP can provide some useful parameters. One is the so-called threshold diameter, which provides a measure of how restricted the ingress of mercury to the interior of the specimen is. This parameter is useful for having a comparative measure of the permeation capacity of the samples. Another parameter is the total pore volume intruded by mercury, which is a measure of the total porosity of the specimen [56]. Finally, MIP can determine the critical pore diameter (CPD), which is defined as the pore diameter that corresponds to the modal pore frequency [57], i.e., the most repeated pore size.

3. Results and discussion

The mixing dosages and procedure to prepare the different pastes are shown in Table 2 and described in the Materials and methods section. As it has been mentioned in other works [44] and observed in our previous work [53] addition of 20 % and higher in volume of MPCMs reduces the workability of the paste and larger amounts of superplasticizer than in the reference pastes had to be added to the mixture to obtain a workable paste. Furthermore, the addition of rGO also dried further the pastes, reducing their workability and therefore the dosage of superplasticizer had to be further increased to obtain good early age workability in the pastes that contain MPCMs and rGO. Good workability was also needed to properly fill the different molds, especially the small crucible for DSC measurement. Nevertheless, this increase in superplasticizer quantity did not delay seemingly the hardening process of the paste and the specimens were hardened enough to be demolded after one day of curing as in standard procedure.

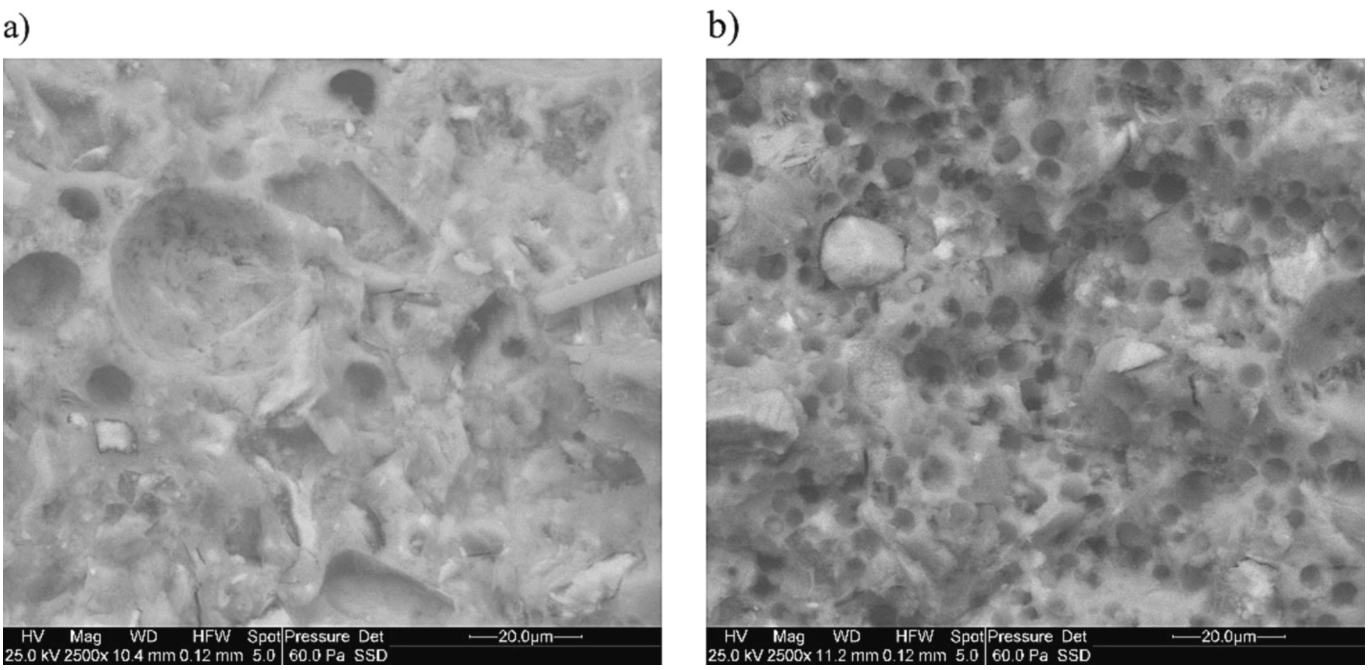

Fig. 3. SEM images of reference paste with 0.3 wt% rGO (based on cement) prepared at the same volume and using the same mixer as for the pastes with MPT25 microcapsules (a) and SEM images of paste with 20 % Vol. MPT25 and rGO (b).

3.1. Morphological and porosity characterization

The different samples were characterized by SEM to analyze the dispersion of the microcapsules, their integrity, and the morphology of the obtained paste. The SEM images of the MPCMs as well as the Centralit metakaolin and the rGO for comparison reasons are shown in the supplementary material (Figs. S3, S4 and S5 respectively). The MRT24 microcapsules range between 1 and 5 µm in size and are visibly agglomerated forming larger spheres (Fig. S3). The Nx24 microcapsules on the other hand are a bit larger in size (between 5 and 40 µm), and they do not tend to agglomerate (see Suppl. Mat., Fig. S3). The size of the MPT25 microcapsules ranges also between 1 and 5 µm as in the case of MRT24 and they also tend to agglomerate according to the SEM images (see Fig. S3). This agglomeration indicates that the shell of the MRT24 and MPT25 are somehow different to the Nx24 shell even though the three of them contain melamine-formaldehyde. This difference can be due to the addition of other compounds that are added to increase the strength of the shell. Moreover, the Centralit metakaolin as well as the rGO were also characterized by SEM to identify them once they were added in the pastes. Metakaolin is made up of sharp particles of various sizes (see Suppl. Mat., Fig. S4). Regarding the rGO, the images show plate like particles that tend to agglomerate (see Suppl. Mat., Fig. S5).

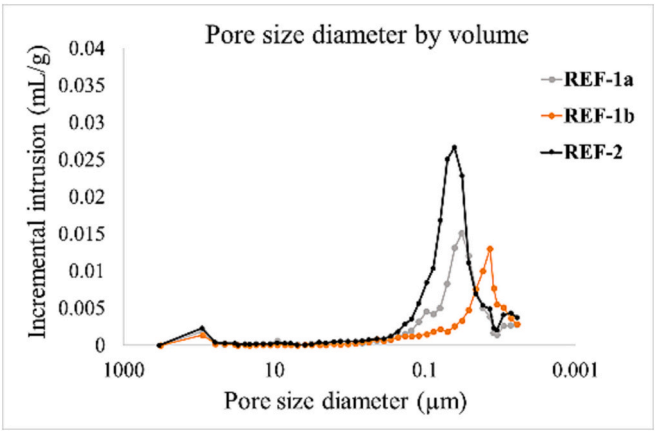

Fig. 4. Pore size distribution of the different reference pastes prepared with the two different procedures. REF-1 (a and b) were prepared at higher mixing speed than REF-2.

In Fig. 1, the images of the reference paste (1a), P1-MRT24 (1b), P1-Nx24 (1c) are shown, while Fig. 2 presents the reference paste, REF-2 (a) and P2-MPT25 (b). In the case of the paste with 20 % in volume of MRT24 (1b), the spherical particles of microencapsulated paraffin dispersed in the matrix can be observed. The microcapsules are well dispersed and distributed in the paste. The entire paste is filled with the microcapsules. In the case of the paste with Nx24 (1c), pores of the size of the microcapsules can be observed as well as the microcapsules. It could be that these micropores are due to the space left by the microcapsules when the specimen was cut to be analyzed it by SEM. This suggests that the interaction between the shell and the paste is poor, and the microcapsules are not attached to the matrix. This result is in contrast with the results obtained with MRT24. In this latter case, there seems to be a better interaction between the shell and cement matrix. This effect could be due to the chemical composition of the polymeric shells as mentioned before, which are slightly different for MRT24 and Nx24. The shell of MRT25 seems to be chemically more compatible with the cement paste than the shell of Nx24. Furthermore, in the case of the paste with Nx24, agglomeration of the microcapsules can also be observed (see Fig. 1c). All the microcapsules have not been well dispersed as it was in the case of the paste with the MRT24. Moreover, in the case of Nx24, larger pores due to air can also be seen in the paste.

In Fig. 2, SEM images of the second reference paste (REF-2) and the pastes with MPT25 are shown. The REF-2 paste shows a higher porosity than REF-1. This could be due to the difference in mixing speed used to prepare both references. The speed was much higher in the REF-1 case which could have helped to get rid of the air bubbles formed in the mixing process. Furthermore, the volume of pastes mixed in the second case (REF-2, P2-rGO, P2-MPT25 and P2-MPT25-rGO) was larger, possibly hindering the release of the air bubbles. In the case of the paste with MPT25 a good dispersion of the microcapsules can be seen. No agglomeration is detected. However, in this case, air pores can also be observed in the paste, which could be a consequence of the mixing process like in the case of the REF-2 paste.

a)

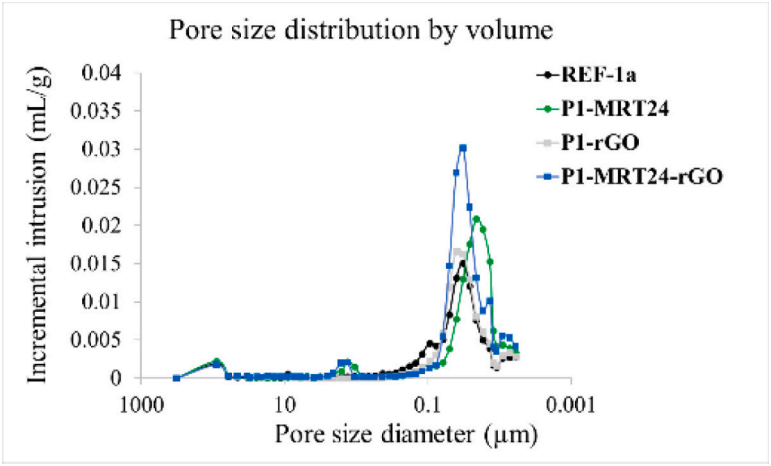

b)

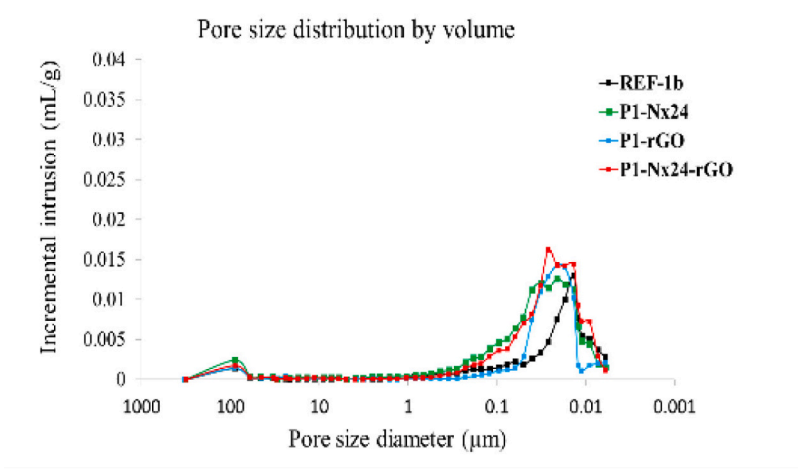

c)

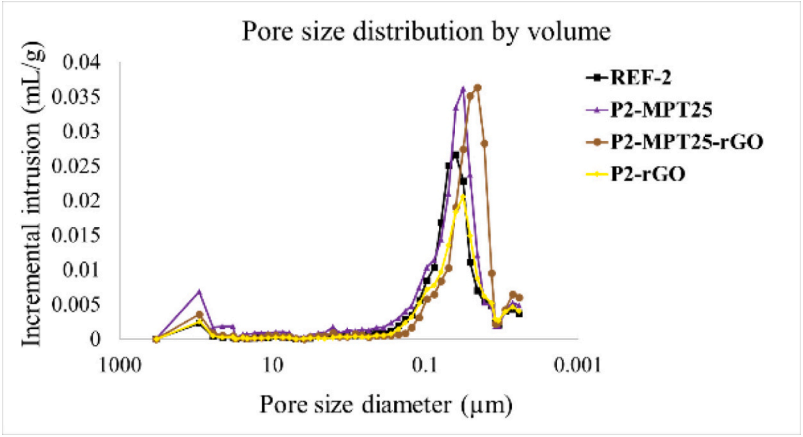

Fig. 5. Pore size distribution by volume of the pastes with the different MPCMs and pastes with MPCMS and rGO compared to their reference. a) REF-1a, P1-MRT24, P1-rGO and P1-MRT24-rGO; b) REF-1b, P1-Nx24, P1-rGO and P1-Nx24-rGO and c) REF-2 and P2-MPT25, P2-rGO and P2-MPT25-rGO.

The SEM images of the pastes with 20 % in Vol. of MPCMs and rGO show similar distribution of the MPCMs (each MPCM-rGO paste analogous to the respective paste-MPCM). Furthermore, the dispersion of the rGO was not observed in the paste. As an example, the SEM images of the paste with 20 % MPT25 and 0.3 wt% rGO are shown in Fig. 3 (the SEM images of the rest of the pastes are included in the Supplementary material, Fig. S6). Image 3a is from the reference paste with rGO (P2-rGO). This paste was prepared using the same volume and the same mixer as in the case of the pastes with MPT25 (which was larger in volume and with lower mixing speed than in the case of the other pastes). No particles of rGO can be observed, but the paste seems to be homogeneous and hydrated. Air pores can also be observed in the paste.

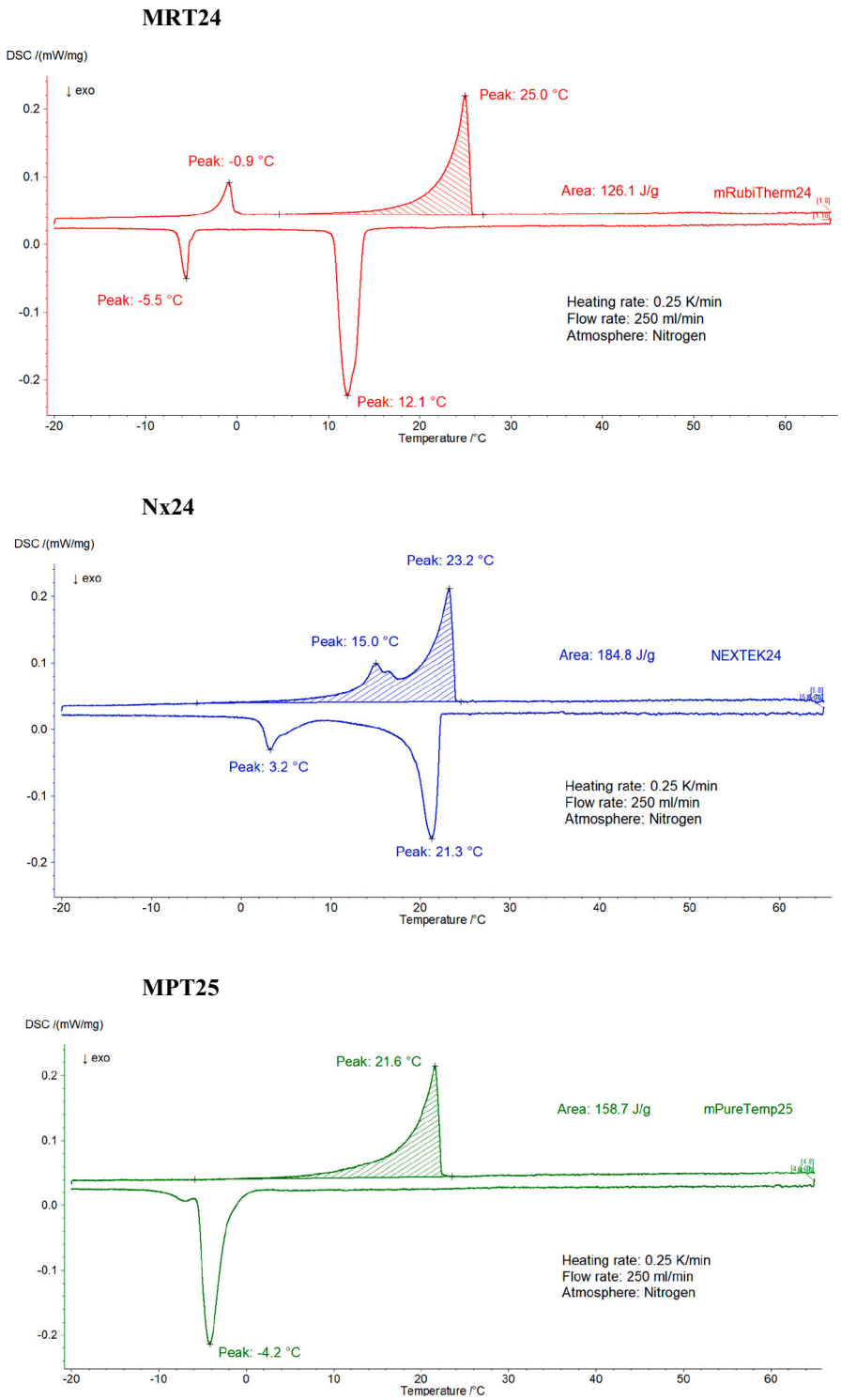

Fig. 6. The DSC thermograms of MRT24, Nx24 and MPT25.

Image 3b shows the paste with MPT25 and rGO (P2-MPT25-rGO). Again, the rGO particles cannot be observed. The microcapsules are well dispersed, similar to the P2-MPT25 paste. As it was mentioned before, these morphologies are very similar to the ones obtained in the pastes with just the MPCM (Fig. 2b).

Mercury intrusion porosimetry, MIP, was carried out to study the pore size distribution and total porosity of the different pastes. In Fig. 4 the pore size distribution of the reference pastes prepared using fast mixing speed (750 rpm, see Materials and methods section) (REF-1a and REF-1b) and lower speed (REF-2) are shown. The REF-2 paste shows a wider pore size distribution than REF-1a and 1b, starting from bigger pore sizes. Furthermore, REF-2 shows a larger porosity than REF-1a and 1b. When comparing REF-1a and REF-1b, they seem to have a similar pore volume although the pore sizes are smaller in the case of REF-1b. This result shows that there is a variability between pastes even though they have the same dosage of the different constituents and they have been mixed in the same way. In Fig. 5 the pore size distribution by volume of all the pastes with respect to their reference paste are shown.

Table 4
Thermal properties of the MPCMs and the corresponding cement pastes without and with rGO measured by DSC. *Data provided by the supplier, in the case of RT24 and Nx24 no heating rate was given.

Samples	T_{Onset} @0.25 °C/min (°C)	T_{Peak} @0.25 °C/min (°C)	Cooling peak temp. @0.25 °C/min	Melting enthalpy (J/g)
RT24*	21*	24*	24*	160
Nx24*	–	24*	–	≥170
PT25*	–	25 (@1 °C/min)	–	≥187
MRT24	13	25	12	125 (@10 K/min)
Nx24	3	23	21	177 (@10 K/min)
MPT25	5	22	−4	153 (@10 K/min)
P1-MRT24	14	25	13	13 (@5 K/min)
P1-MRT24-rGO	14	25	13	14 (@5 K/min)
P1-Nx24	10	25	23	19 (@5 K/min)
P1-Nx24-rGO	10	25	23	19 (@5 K/min)
P2-MPT25	10	21	12	17 (@5 K/min)
P2-MPT25-rGO	11	21	12	17 (@5 K/min)

In all cases, when the MPCMs are added, the porosity of the pastes increases. In the case of the pastes with just the rGO, no significant change can be observed with respect to the reference paste. In general terms, these results agree with the images of the different pastes obtained by SEM (see Figs. 1, 2 and 3).

In conclusion, the trend observed with the samples containing MPCMs and rGO compared to their reference shows that the addition of the rGO does not change the morphology of the paste, whereas the addition of MPCMs increases the porosity in all cases and in particular in the case of Nx24, where the size distribution shifts to slightly higher sizes, confirming the observations done by SEM. Similar results have been reported in the literature. For example, Sam et al. [45] found that the overall porosity increased when MPCM (in their case Nextek 37D) was added and when its quantity was increased. Furthermore, the addition of MPCM changed the pore size/structure of the paste.

3.2. Characterization of thermal and electrical properties

3.2.1. Thermal properties

DSC tests were carried out on the microencapsulated PCMs as well as the cement-MPCM and cement-MPCM-rGO composites to study the possible effects that the microencapsulation and rGO might have on the thermal properties. In Fig. 6, the DSC thermograms of the three microencapsulated PCMs (MRT24, Nx24 and MPT25) are shown. Both MRT24 and Nx24 show two phase change transition peaks, one with a lower latent heat than the other one. In the case of MRT24, the peak temperature of the lower latent phase change is around 1 °C, whereas the larger latent heat melting transition is around 25 °C (main peak). In the cooling phase, both transition phases are observed but shifted to lower temperatures (temperature peaks at 12 °C and −6 °C). MRT24 shows a relatively large hysteresis between the heating and cooling process. This differs from the results of the phase change transition temperatures of the raw material obtained by Sam et al. [25] and the ones provided by the supplier (see Table 4). Sam et al. report a peak heating temperature of 25 °C (24 °C in the case of the supplier) for the main melting peak, which is similar to the peak temperature obtained for the microencapsulated RT24 in this study. However, the peak cooling temperature they reported is 23.8 °C (24 °C provided by the supplier) which is significantly higher than the one measured for the MRT24 in this study (12 °C). This could indicate that the microencapsulation affects the thermophysical properties of the PCM. In fact, studies can be found in the literature where the authors report changes in the thermal response of the PCMs due to encapsulation [46].

In the case of Nx24, a complex peak with two clear peak temperatures can be observed (Fig. 6). For the heating, the first one around 15 °C, and the second around 23 °C. In the cooling process, the main transition occurs around 21 °C (similar to the temperature in the heating process), however the second transition shifts to much lower temperatures (around 3 °C), resulting in a very broad recrystallization peak. In this case, the main phase change transition, which could be of interest for building applications, does not show a large hysteresis as opposed to the MRT24 case. For this MPCM, no comparison to the raw PCM material could be carried out since the product was acquired microencapsulated. Eventually, the data provided by the supplier corresponds to the assessed results in this study. In the case of MPT25, only one phase transition can be seen in the heating process with a peak temperature at 22 °C. However, in this case, the phase change transition shifts considerably in the cooling process. A double peak is observed, with a main peak temperature at −4 °C and a small shoulder at −7 °C. This is quite different to the results obtained for the raw material by Sam et al. [25] and verified by the authors, where the peak temperatures of the heating and cooling were showing only low hysteresis ($T_{peak\ heating} = 25.4$ °C and $T_{peak\ cooling} = 21.1$ °C) and no additional peaks were observed. This again shows that microencapsulation could modify the thermophysical response of the material. It should be pointed out that the MPT25 shows the largest hysteresis of all the MPCMs studied in this work between the heating and the cooling process.

In Table 4, the peak melting temperatures and the latent heat of the microencapsulated PCMs calculated from the DSC thermograms are shown. In the MRT24 and MPT25 cases, the melting enthalpy is slightly lower than in the case of the raw material. This is normal since the microencapsulated product is not 100 % PCM and contains both the PCM and the polymeric shell. From the obtained enthalpies, it is possible to estimate the weight percentage of PCM in the microencapsulated product. In the case of MRT24, the melting enthalpy is around 125 J/g, which indicates a PCM content of ca. 78 % and for the MPT25 the melting enthalpy is 153 J/g pointing to a PCM content of ca. 82 %. In the case of Nx24, the peak temperature is very similar to the one given by the provider, which is expected since the product is already microencapsulated.

The different cement pastes with MPCMs and rGO were also characterized by DSC to measure the phase transition temperature in the heating and cooling process as well as the melting enthalpy of the pastes. The latter is one of the main aspects of the current research, which aims to study the appropriateness of the different MPCMs to be used in cement-based panels for building applications. In Fig. 7, the thermograms of the pastes with 20 % MRT24, Nx24 and MPT25 are shown. In Table 4 the temperature onset, the heating and cooling peak temperatures and melting enthalpy of all the pastes can be found. Nevertheless, as MPCMs transitions occur over broad temperature ranges, with several transitions overlaying, the onset temperatures cannot be precisely determined. The latter are then reported for information, but the peak temperatures have been retained as reference for the transition temperatures in the following. P1-MRT24 and P1-Nx24 show similar phase transition peaks (at similar heating and cooling peak temperatures) as the equivalent MPCMs but with lower melting enthalpy since the MPCMs are in a dosage of 20 % Vol. in the whole composite. However, in the case of the P2-MPT25 the thermogram is different, especially in the cooling part, to the thermogram shown by the MPT25. In the cooling process, two main peaks can be observed at different temperatures, one

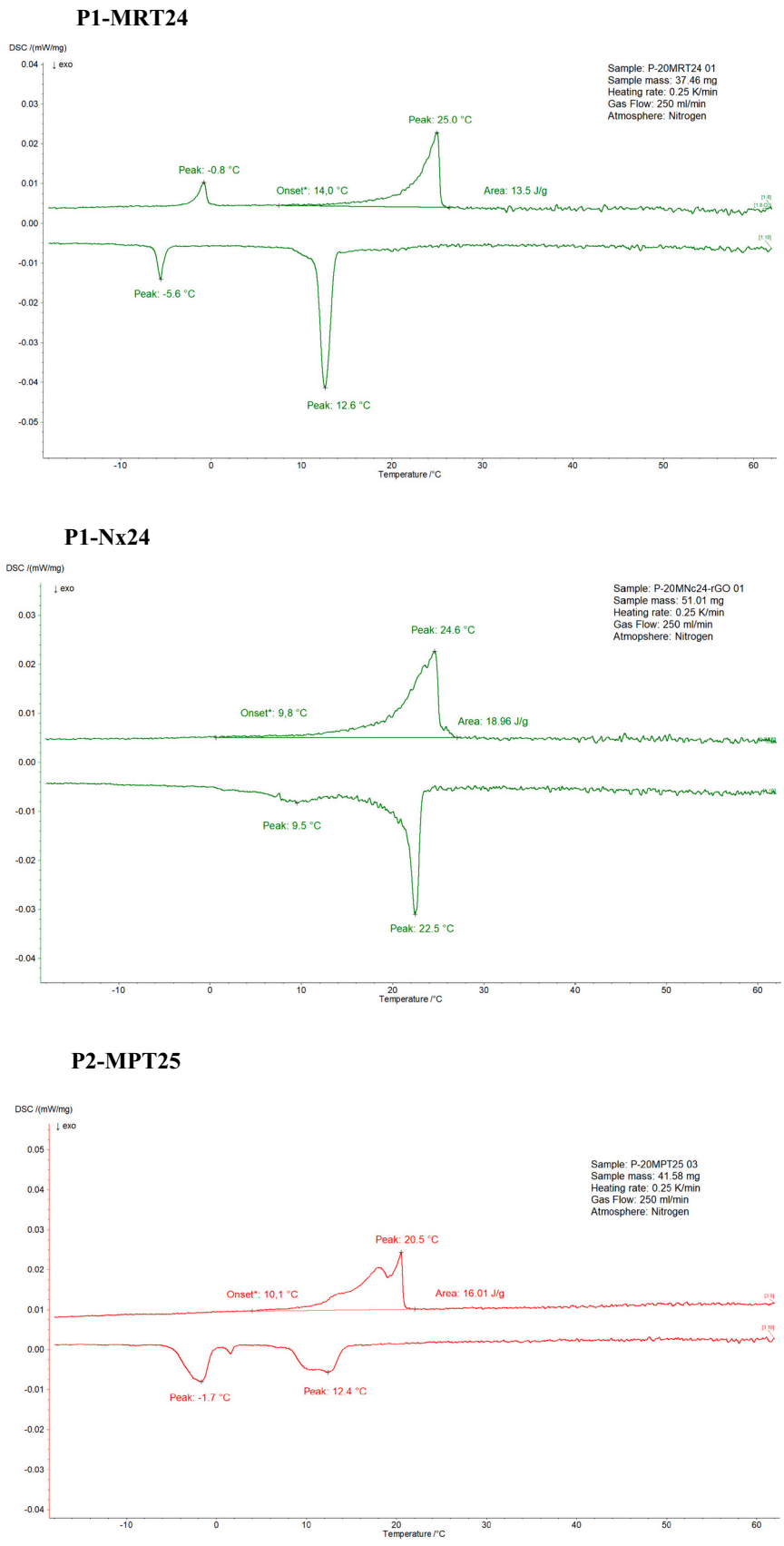

Fig. 7. DSC thermograms of cement pastes with 20 % vol. of MRT24, Nx24 and the bio-PCM MPT25.

Table 5
Thermal conductivities at 5 and 35 °C of MPCMs, rGO, pure cement paste at w/b ratio of 0.33 and pastes with and without rGO and three types of MPCMs. *The pellets of Nx24 (made to measure thermal conductivity) lose their shape and disintegrate, making it impossible to do the measurement.

Samples	Thermal conductivity (W/m/K) @5 °C	Thermal conductivity (W/m/K) @35 °C
	Average value	Average value
rGO	0.518 @20 °C	
MRT24	0.145	0.111
Nx24	0.2677	N.A.*
MPT25	0.296	0.243
REF-1a	0.947	0.880
P1-rGO	0.869	0.838
P1-RT24	0.750	0.698
P1-RT24-rGO	0.723	0.698
REF-1b	0.918	0.866
P1-Nx24	0.73	0.673
P1-Nx24-rGO	0.725	0.666
REF-2	0.732	0.713
P2-rGO	0.773	0.754
P2-PT25	0.600	0.578
P2-PT25-rGO	0.551	0.547

at 12 °C and the other one at around −1 °C.

It should be pointed out that the phase transition at 12 °C found in the paste did not appear in the MPT25 thermogram. It is not very clear the reason for this effect, but it indicates the importance of analyzing the thermophysical properties of all the composites since unexpected behavior can be observed. The second largest peak in the cooling process is around −1 °C similar to the one found in the MPT25 thermogram and another small peak is also observed at 1 °C. It should be underlined that due to the peak at 12 °C, the hysteresis between the heating and cooling peak is much lower in the case of the paste compared to the just MPT25 thermogram. Similar results were obtained in all pastes with the addition of rGO (see Supplementary material, Fig. S7).

When the different pastes are compared, the largest melting enthalpy was observed in the pastes with 20 % Vol. Nx24D, which was expected since for the same amount of mass the microencapsulated Nx24 showed a higher heat storage capacity than the other microencapsulated PCMs. The second largest thermal enthalpy is shown by the pastes with MPT25, followed by the pastes with MRT24. The highest difference between melting and cooling temperature peaks is observed for the pastes containing MRT24 and MPT25. Interestingly, the P-MPT25 pastes have a narrower temperature difference peaks than expected (taking into account the temperature difference between melting and solidifying shown by the MPT25 on its own). In terms of latent energy storage, the microencapsulated Nx24 give the best results, followed by the MPT25. The Nx24 also shows the lowest difference between heating and cooling peaks. In general, the addition of rGO does not have a large effect on the latent heat (see Suppl. mat., Fig. S7).

3.2.2. *Thermal conductivity and thermal diffusivity*

In addition to a high energy storage capacity, thermal conductivity and/or diffusivity are important parameters for assessing the ability of a cement paste/PCM mixture to store and release this energy quickly. In order to modify these parameters and thus obtain a more versatile final mixture, rGO was added to the pastes. The thermal conductivities of the pastes, without and with rGO, were characterized by the transient hot disk method and their thermal diffusivity by the laser flash technique. In the literature, high electrical and thermal conductivities (e.g., between 30 and 2600 Wm^{-1} K^{-1}) have been published for rGO thin films [48], but these types of materials show an anisotropic behavior, that is, the thermal conductivity of the material varies depending on the direction (in-plane or cross-plane) of conduction, usually having a high

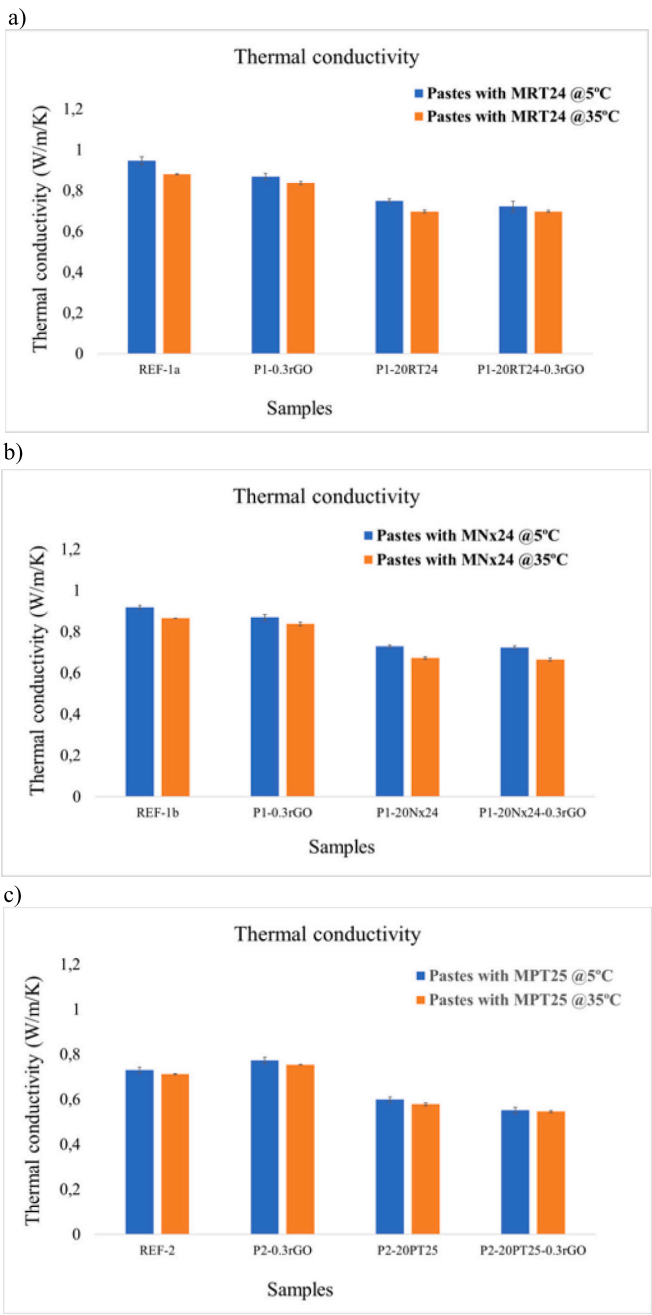

Fig. 8. a) Thermal conductivity data obtained for the pastes with MRT24 with and without rGO compared to their reference paste; b) Thermal conductivity measured for the pastes with Nx24 with and without rGO compared to their reference paste; c) Thermal conductivity data obtained for the pastes with MPT25 with and without rGO compared to their reference paste.

conductivity in the in-plane direction and much lower in the cross-plane direction [49]. For example, Renteria et al. [49] measured an in-plane thermal conductivity of 61 Wm^{-1} K^{-1} and a cross-plane thermal conductivity of ~0.09 Wm^{-1} K^{-1} in reduced graphene oxide films annealed at temperatures up to 1000 °C.

Table 5 summarizes the results obtained for the different cement pastes with MPCM and rGO. This table shows the very good reproducibility of the tests with a maximum standard deviation of 4 % of the different average values (1 % in average). In addition, the adequacy of the method was assessed by studying the residuals between the experimental thermograms of all the tests carried out and the theoretical model. In all cases, these residues can be assimilated to white noise,

Table 6
Thermal diffusivity of the pastes characterized by LFA and estimated by the Hot-Disk measurements.

Samples	Ther. Diff. (mm^2/s) LFA @5 °C	Ther. Diff. (mm^2/s) HD @5 °C	Ther. Diff. (mm^2/s) LFA @35 °C	Ther. Diff. (mm^2/s) HD @35 °C
	Average value	Average value	Average value	Average value
REF-1a	0.388	0.4138	0.365	0.3222
P1-rGO	0.379	–	0.352	–
P1-MRT24	0.29	0.3381	0.274	0.2921
P1-MRT24-rGO	0.295	0.3145	0.249	0.2789
REF-1b	0.395	0.5042	0.372	0.35
P1-rGO	0.371	0.4709	0.352	0.3675
P1-Nx24	0.33	0.3604	0.278	0.2994
P1-Nx24-rGO	0.317	0.3615	0.263	0.2991
REF-2	0.339	0.3362	0.319	0.2887
P2-rGO	0.322	0.3430	0.304	0.2894
P2-MPT25	0.272	0.2810	0.261	0.2457
P2-MPT25-rGO	0.282	0.2768	0.264	0.2579

centred on zero and of low amplitude (about 200 μK for a total temperature rise of about 2 K).

Besides the pastes, the thermal conductivity of the MPCMs as well as the rGO was also characterized. The microencapsulated PCMs show expected thermal conductivities. For example, the thermal conductivity of RT24 is reported to be 0.2 Wm^{-1} K^{-1} [36], and in the case of PT25, 0.15 Wm^{1}_{-} K^{-1} for liquid phase and 0.25 W/m^{-1} K^{-1} for solid phase [38], all similar to the results obtained for the microencapsulated PCMs in the current study. The rGO also shows a low thermal conductivity, although it is larger than the ones shown by MPCMs. It is important to mentioned that this low conductivity is probably due to the fact that the prepared rGO pellet for the measurement is formed by randomly distributed platelets (i.e., not ordered) and because of their strongly anisotropic thermal conductivity behavior, the average thermal conductivity measured is low.

In Fig. 8, the thermal conductivities measured at 5 °C and 35 °C are plotted. Fig. 8a shows the thermal conductivities of the pastes with MRT24 with and without rGO, Fig. 8b shows the conductivity of the pastes with Nx24, with and without rGO and Fig. 8c shows the thermal conductivities of pastes with MPT25 with and without rGO.

Strong variation in thermal conductivity can be observed between REF-1 (a and b) and REF-2 which is probably due to the larger porosity in REF-2. Nevertheless, the trend is similar in all the pastes when the MPCMs are added. The thermal conductivities of the cement pastes decrease when MPCMs are added, between 17 and 29 %. This result was expected since the MPCMs have lower thermal conductivity [36,38] than the paste (Table 5), leading to an overall decrease in the effective thermal conductivity of the mixture. Unfortunately, the addition of rGO has no significant impact on thermal conductivity of the cement pastes, although it generally tends to slightly reduce the effective thermal conductivity of the mixture (up to 8 %) except in the case of paste 2 where it increases slightly. This could be due to the fact that the addition of rGO to REF-2 decreases somewhat the porosity (see Fig. 5c). The low thermal conductivity could be due to a bad dispersion of the rGO particles. Regarding the type of MPCM used, no significant impact was observed; on average the resulting effective thermal conductivities decrease of ca. 20 % when compared to the corresponding reference cement paste. Nevertheless, it should be noted that the combination of MPT25 and rGO leads to a significant decrease of ca. 29 % of the thermal conductivity of the cement paste. The SEM images and porosimetry in Section 2.1 can explain this variation by the higher porosity of this mixture compared to the other ones. Finally, the thermal conductivities of the cement pastes tend to decrease when temperature increases, a behavior already reported in literature [50].

LFA was used to determine the thermal diffusivity of the pastes at the same temperatures (5 °C and 35 °C). They were compared to the ones estimated through the Hot-Disk thermal conductivity measurements. In Table 6 the thermal diffusivity values obtained with LFA and the ones estimated by Hot-Disk are shown. Furthermore, the results obtained by LFA of the different pastes are plotted in Fig. 9.

In general terms, the thermal diffusivity estimated by Hot-Disk is slightly higher than the ones measured by LFA. The results show that the thermal diffusivity decreases with the addition of the MPCMs. Overall, the diffusivity is reduced between 16 % and 25 % at both temperatures when MPCMs are added. The thermal diffusivity shown by the REF-2 paste is slightly smaller than the other references, but the reduction when MPT25 is added follows the same trend as the other pastes. Furthermore, the diffusivity is reduced with temperature increase. The addition of rGO does not increase the diffusivity. These results are very similar to the ones obtained for thermal conductivity.

3.2.3. *Electrical conductivity*

Electrical conductivity of the pastes was also measured by broadband dielectric spectrometer to evaluate the effect of the added rGO. The electrical conductivity was measured at room temperature in the frequency range 0.2 Hz to 1 MHz. Fig. 10 shows the electrical conductivity of the pastes as a function of frequency with the different MPCMs and with and without rGO. The electrical conductivity of the reference pastes measured at 50 Hz ranges between 2.1e-10 and 2.5e-9 S/cm. These are low conductivities, and it is probably due to the movement of ions found in the water within the pores of the paste [51,52]. Electrical conductivity of rGO at 42 °C was measured to be 1.0e-2 S/cm. The electrical conductivity of the reference pastes are around 8 orders of magnitude lower than the conductivity of rGO. Since electrical conductivity of rGO is many orders of magnitude higher than a cement paste, it was expected to see an improvement of this property in the cement paste mixed with rGO. Unfortunately, this was not the case and in fact, the addition of the rGO does not have much effect in the conductivity of the pastes and are similar to the reference pastes. Furthermore, addition of 20 % of MRT24 and Nx24 with and without rGO does not seem to change much the electrical conductivity of their pastes either. Only in the case of pastes with MPT25, a larger increase of electrical conductivity can be observed, especially in the paste with both additions (MPT25 and rGO), where the electrical conductivity increases two orders of magnitude compared to the reference paste.

However, these conductivities are still quite low and in the range of ionic conductivity. The conductivity is probably due to the movement of ions found in the water in the pores. These results suggest that the rGO is probably not well dispersed in the matrix and therefore an increase in electrical conductivity is not observed. It is well known that graphene besides being hydrophobic, it tends to agglomerate, and different dispersion techniques can be found in the literature [58]. Because of that, the main purpose of synthesizing a reduced graphene oxide and adding it as a water dispersion to the cement paste was to improve the dispersion in the cement matrix. However, it seems that a good dispersion of the rGO was not achieved in this case.

a)

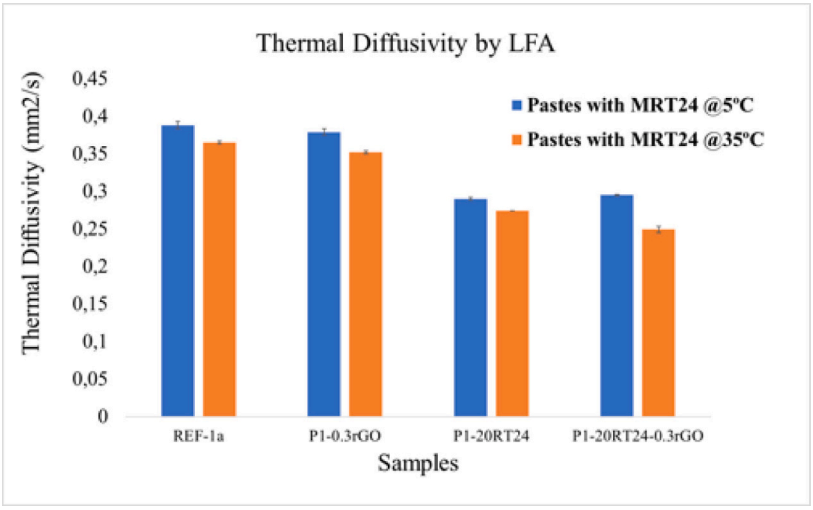

b)

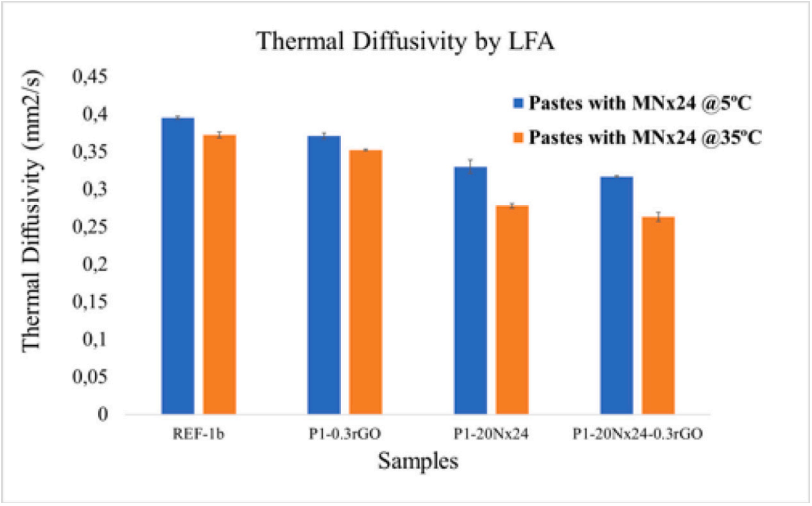

c)

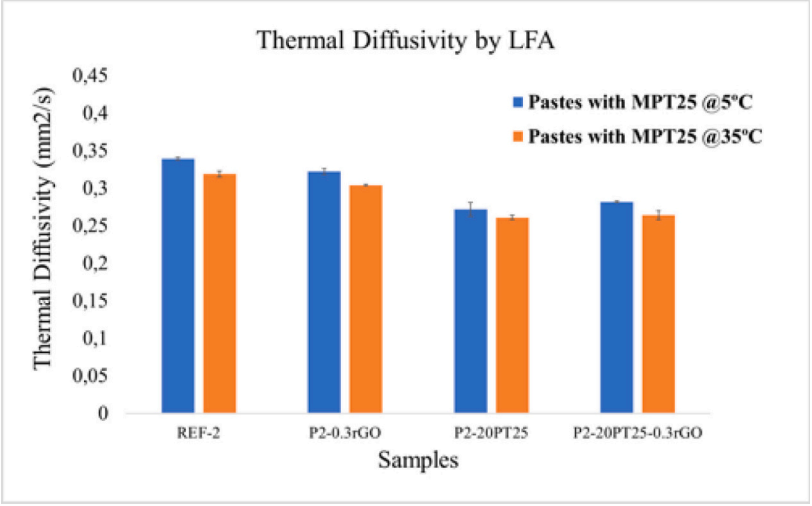

Fig. 9. Thermal diffusivity measured by LFA at 5 °C and 35 °C of pastes with 20 % Vol. MRT24 with and without rGO (a); pastes with 20 % Vol. Nx24 with and without rGO (b) and pastes with 20 % Vol. MPT25 with and without rGO (c).

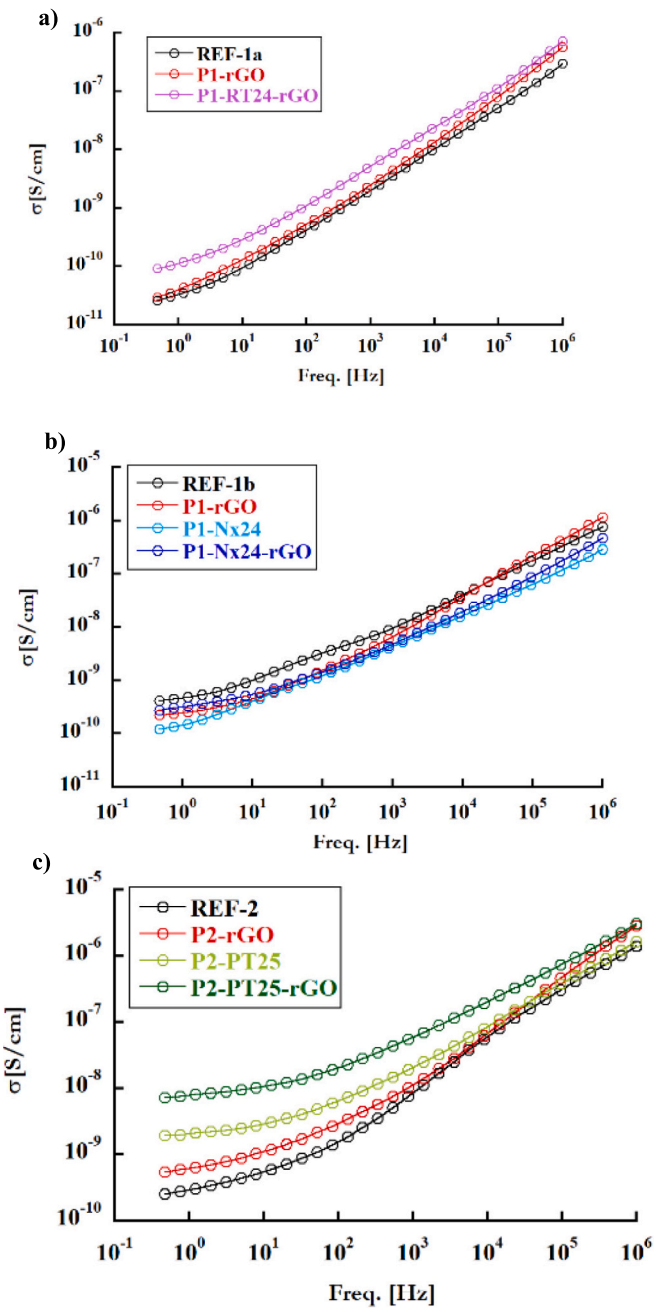

Fig. 10. Electrical conductivity measured at room temperature and different frequencies of a) pastes with MRT24 and rGO (it was not possible to obtain the electrical conductivity of P1-MRT24 because the sample broke during the measurement); b) pastes with Nx24 with and without rGO and c) pastes with MPT25 with and without rGO.

4. Conclusions

Cement pastes that contain 20 % in Vol. of three different micro-encapsulated phase change materials (two paraffin based, RubiTherm24 and Nextek24, and one bio-based, PureTemp25) have been cast with a water/binder ratio of 0.33. Furthermore, with the goal of improving the charge/discharge response of the MPCM-pastes, 0.3 wt% reduced graphene oxide (rGO) was added, and the characterization of the thermal and electrical properties, as well as the energy storage capacity of all the pastes was carried out, including the comparison between them. Moreover, the morphology of the pastes as well as the pore size distribution have been characterized by scanning electron microscopy and mercury intrusion porosimetry. Two different paste volumes and mixing procedures have been used to prepare the pastes. Cement pastes that contain RubiTherm24 (MRT24) and Nextek 24D (Nx24) were mixed at smaller mortar volume and higher speed than the pastes prepared with PureTemp25 (MPT25), which were done at higher mortar volume and slower mixing speed with the aim of analyzing the scaling up of the mixing procedure. This difference had an effect in the final porosity of the pastes. Overall, the pastes mixed at higher speed showed a lower porosity than the ones prepared at lower speed. As it was mentioned, the addition of the MPCMs as well as rGO, has worsen the workability of the pastes, and the use of a less powerful mixing could have produced a more porous final paste. These results should be considered when designing the scaling up of the process to produce large amount of material.

Differences in the Differential Scanning Calorimeters thermograms between the microencapsulated PCM (MRT24 and MPT25) and the raw PCM were observed. In both cases, the cooling peak temperature of MPCM is much lower than in the raw PCM (according to data from the supplier and [45]). This delay in phase change transition might be due to the insulating effect of the shell. This result indicates that microencapsulation can modify thermophysical properties of the PCMs. In the case of the DSC thermograms of the pastes with MPCMs, with and without rGO, they are very similar to the ones shown by the microencapsulated PCMs, except in the case of MPT25. In the latter, the paste with MPT25 (with and without rGO) shows a similar heating peak temperature, but the cooling peak temperature is higher than in the case of just MPT25 (12 °C vs −4 °C). It is not clear the reason of this result. However, it suggests that in order to choose the right PCM for the thermal energy storage (TES) application it is not only important to know the thermophysical properties of the PCMs but also the response when they are microencapsulated and embedded in the material chosen for the TES system.

Regarding the melting enthalpy, all the pastes have a similar melting enthalpy, although the largest is shown by the paste which contains Nx24 (19 J/g) followed by the paste with the bio-PCM MPT25 (17 J/g), and finally by the paste with MRT24 (13 J/g). This was expected since the microencapsulated PCM that showed the largest melting enthalpy was Nx24 followed by MPT25 and then by MRT24. All samples show displacement between melting and cooling peaks, being the largest one shown by the pastes that contained MRT24, followed by the pastes with MPT25 microcapsules. The lowest displacement was shown by the pastes with Nx24.

Regarding the thermal conductivity and diffusivity, the reference paste with higher porosity (REF-2) has a lower thermal conductivity and lower diffusivity compared to the other reference pastes (REF1a and REF1b). This could be due to the larger porosity shown by REF-2. However, all the pastes showed similar trend when MPCMs were added, i.e., their addition reduced even more the thermal conductivity and diffusivity of the composites. Furthermore, the addition of rGO does not have a significant impact on thermal conductivity and diffusivity. The low thermal conductivity could be due to a bad dispersion of the rGO micro/nanoplatelets. Furthermore, rGO shows anisotropy in thermal conductivity, having a larger conductivity in one direction (in-plane) opposed to the other one (cross-plane) [49]. Therefore, a bad and random distribution of the platelets could end up showing an average low thermal conductivity in the whole paste. Moreover, the bad dispersion could also be the reason for the low electrical conductivities obtained when rGO was added to the different MPCMs pastes. It must also be mentioned that in the current work the measurements of thermal diffusivity carried out by both methods, Hot-Disk and Laser Flash technique (LFA), are in good agreement. These results validated the Hot-Disk as a good method for determining thermal diffusivity of these materials.

To conclude, regarding heat capacity, the best MPCM is the paraffin based Nx24 (highest thermal enthalpy and lowest peak temperature displacement between melting and cooling), whereas the biobased

MPT25 shows the next best behavior, but with a larger displacement between heating and cooling peaks, this being no good for obtaining complete heat absorption and release cycles (at similar room temperature). The current study underscores the importance of fully characterizing and having information of the thermal properties of all the elements (raw PCMs, MPCMs and their combination with cement composites) in order to be able to evaluate the best PCM options for the application sought for.

CRediT authorship contribution statement

E. Erkizia: Investigation, Writing – original draft, Writing – review & editing. **C. Strunz:** Investigation, Writing – original draft, Writing – review & editing. **J.L. Dauvergne:** Investigation, Writing – original draft, Writing – review & editing. **G. Goracci:** Investigation, Writing – original draft, Writing – review & editing. **I. Peralta:** Conceptualization, Investigation, Supervision, Writing – original draft, Writing – review & editing. **A. Serrano:** Investigation, Writing – review & editing. **A. Ortega:** Investigation, Writing – original draft, Writing – review & editing. **B. Alonso:** Investigation, Writing – review & editing. **F. Zanoni:** Investigation, Writing – original draft, Writing – review & editing. **M. Düngfelder:** Investigation, Writing – review & editing. **J.S. Dolado:** Conceptualization, Investigation, Supervision, Writing – review & editing. **J.J. Gaitero:** Conceptualization, Investigation, Supervision, Writing – review & editing. **C. Mankel:** Conceptualization, Investigation, Supervision, Writing – review & editing. **E. Koenders:** Conceptualization, Investigation, Supervision, Writing – review & editing.

Declaration of competing interest

The authors declare that they have no known competing financial interests or personal relationships that could have appeared to influence the work reported in this paper.

Data availability

Data will be made available on request.

Acknowledgements

All the authors gratefully acknowledge the financial support from the NRG-STORAGE project (870114, 2020-2024, https//nrg-storage.eu/), financed by the European Union H2020 Framework under the LC-EEB-01-2019 call, IA type.

J. S. Dolado acknowledges the funds from the project PoroPCM (PCI2019-103657) funded by MCIN/AEI/10.13039/50110001133 and co-funded by the European Union (Programación Conjunta Internacional 2019).

J. S. Dolado, G. Goracci, J. J. Gaitero and E. Erkizia would like to acknowledge the Laboratory for Transborder Cooperation "Aquitaine-Euskadi Network in Green Concrete and Cement-based Materials" (LTC-Green Concrete).

Appendix A. Supplementary data

Supplementary data to this article can be found online at https://doi.org/10.1016/j.est.2024.110675.

References

[1] C. Fabiani, A.L. Pisello, A. D'Alessandro, F. Ubertini, L.F. Cabeza, F. Cotana, Effect of PCM on the hydration process of cement-based mixtures: a novel thermos-mechanical investigation, Materials 11 (2018) 871–888, https://doi.org/10.3390/ma11060871.

[2] Z. She, Z. Wei, B.A. Young, G. Falzone, N. Neithalath, G. Sant, L. Pilon, Examining the effects of microencapsulated phase change materials on early-age temperature evolutions in realistic pavement geometries, Cem. Concr. Compos. 103 (2019) 149–159, https://doi.org/10.1016/j.cemconcomp.2019.04.002.

[3] H.G. Kim, A. Qudoos, I.K. Jeon, B.H. Woo, J.S. Ryon, Assessment of PCM/SiC-based composite aggregate in concrete: energy storage performance, Construct. Build Mater. 258 (2020) 119637, https://doi.org/10.1016/j.conbuildmat.2020.119637.

[4] Y. Tian, Y. Lai, Z. Qin, H. Li, Study on the physical mechanical properties and freeze-thaw resistance of artificial phase change aggregates, Construct. Build Mater. 329 (2022) 127225, https://doi.org/10.1016/j.conbuildmat.2022.127225.

[5] J.H. Yeon, Thermal behavior of cement mortar embedded with low-phase transition temperatures PCM, Construct. Build Mater. 252 (2020) 119168, https://doi.org/10.1016/j.conbuildmat.2020.119168.

[6] S. Pilehvar, A.M. Szczotok, J.F. Rodríguez, L. Valentini, M. Lanzón, R. Pamies, A.-L. Kjøniksen, Effect of freeze-thaw cycles on the mechanical behavior of geopolymer concrete and Portland cement concrete containing micro-encapsulated phase change materials, Construct. Build Mater. 200 (2019) 94–103, https://doi.org/10.1016/j.conbuildmat.2018.12.057.

[7] B. Lamrani, K. Johannes, F. Kuznik, Phase change materials integrated into building walls: an updated review, Renew. Sustain. Energy Rev. 140 (2021) 110751, https://doi.org/10.1016/j.rser.2021.110751.

[8] N. Soares, J.J. Costa, A.R. Gaspar, P. Santos, Review of passive PCM latent heat thermal energy storage systems towards buildings' energy efficiency, Energ. Buildings 59 (2013) 82–103, https://doi.org/10.1016/j.enbuild.2012.12.042.

[9] C. Li, H. Yu, Y. Song, Experimental investigation of thermal performance of microencapsulated PCM-contained wallboard by two measurement modes, Energ. Buildings 184 (2019) 34–43, https://doi.org/10.1016/j.enbuild.2018.11.032.

[10] F.E. Boudali, S. Chikh, L. Derradji, Experimental and numerical investigation for improving the thermal performance of a microencapsulated phase change material plasterboard, Energ. Conver. Manage. 174 (2018) 309–321, https://doi.org/10.1016/j.enconman.2018.08.052.

[11] A. Oliver, Thermal characterization of gypsum boards with PCM included: thermal energy storage in buildings through latent heat, Energ. Buildings 48 (2012) 1–7, https://doi.org/10.1016/j.enbuild.2012.01.026.

[12] C. Li, H. Yu, Y. Song, Z. Liu, Novel hybrid microencapsulated phase change materials incorporated wallboard for year-long year energy storage in buildings, Energ. Conver. Manage. 183 (2019) 791–802, https://doi.org/10.1016/j.enconman.2019.01.036.

[13] R. Barzin, J.J.J. Chen, B.R. Young, M.M. Farid, Application of PCM underfloor heating in combination with PCM wallboards for space heating using price based control system, Appl. Energy 148 (2015) 39–48, https://doi.org/10.1016/j.apenergy.2015.03.027.

[14] F. Guarino, A. Athienitis, M. Cellura, D. Bastien, PCM thermal storage design in buildings: experimental studies and applications to solaria in cold climates, Appl. Energy 185 (2017) 95–106, https://doi.org/10.1016/j.apenergy.2016.10.046.

[15] P. Devaux, M.M. Farid, Benefits of PCM underfloor heating with PCM wallboards for space heating in winter, Appl. Energy 191 (2017) 593–602, https://doi.org/10.1016/j.apenergy.2017.01.060.

[16] D. Zhou, Y. Tian, Y. Qu, Y.K. Chen, Thermal analysis of phase change material board (PCMB) under weather conditions in the summer, Appl. Therm. Eng. 99 (2016) 690–702, https://doi.org/10.1016/j.applthermaleng.2016.01.121.

[17] A. Fateh, D. Borelli, F. Devia, H. Weinläder, Summer thermal performances of PCM-integrated insulation layers for light-weight building walls: effect of orientation and melting point temperature, Thermal Science and Engineering Progress 6 (2018) 361–369, https://doi.org/10.1016/j.tsep.2017.12.012.

[18] I. Mandilaras, M. Stamatiadou, D. Katsourinis, G. Zannis, M. Founti, Experimental thermal characterization of a Mediterranean residential building with PCM gypsum board walls, Build. Environ. 61 (2013) 93–103, https://doi.org/10.1016/j.buildenv.2012.12.007.

[19] K.O. Lee, M.A. Medina, X. Sun, On the use of plug-and-play walls (PPW) for evaluating thermal enhancement technologies for building enclosures: evaluation of a thin phase change material (PCM) layer, Energ. Buildings 86 (2015) 86–92, https://doi.org/10.1016/j.enbuild.2014.10.020.

[20] A. Frazzica, V. Brancato, V. Palomba, D. La Rosa, F. Grungo, L. Calabrese, E. Proverbio, Thermal performance of hybrid cement mortar-PCMs for warm climates application, Sol. Energy Mater. Sol. Cells 193 (2019) 270–280, https://doi.org/10.1016/j.solmat.2019.01.022.

[21] P. Arce, C. Castellón, A. Castell, L.F. Cabeza, Use of microencapsulated PCM in buildings and the effect of adding awnings, Energ. Buildings 44 (2012) 88–93, https://doi.org/10.1016/j.enbuild.2011.10.028.

[22] A. Castell, M.M. Farid, Experimental validation of a methodology to assess PCM effectiveness in cooling building envelopes passively, Energ. Buildings 81 (2014) 59–71, https://doi.org/10.1016/j.enbuild.2014.06.011.

[23] B.A. Young, G. Falzone, Z. Wei, G. Sant, L. Pilon, Reduced-scale experiments to evaluate performance of composite building envelopes containing phase change materials, Construct. Build Mater. 162 (2018) 584–595, https://doi.org/10.1016/j.conbuildmat.2017.11.160.

[24] G. Simonsen, R. Ravotti, P. O'Neill, A. Stamatiou, Biobased phase change materials in energy storage and thermal management technologies, Renew. Sustain. Energy Rev. 184 (2023) 113546, https://doi.org/10.1016/j.rser.2023.113546.

[25] M.N. Sam, A. Caggiano, C. Mankel, E. Koenders, A comparative study on the thermal energy storage performance of bio-based and paraffin-based PCMs using DSC procedures, Materials 13 (2020) 1705, https://doi.org/10.3390/ma13071705.

[26] C. Mankel, A. Caggiano, N. Ukrainczyk, E. Koenders, Thermal energy storage characterization of cement-based systems containing microencapsulated-PCMs, Construct. Build Mater. 199 (2019) 307–320, https://doi.org/10.1016/j.conbuildmat.2018.11.195.

[27] P. Singh, R.K. Sharma, A.K. Ansu, R. Goyal, Study of thermal properties of organic phase change materials for energy storage, Materials Today: Proceedings 28 (2020) 2353–2357, https://doi.org/10.1016/j.matpr.2020.04.640.
[28] A.G. Olabi, T. Wilberforce, K. Elsaid, E.T. Sayed, M. Ramadan, S.M.A. Rahman, M. A. Abdelkareem, Recent progress on carbon-based nanomaterial for phase change materials: prospects and challenges, Thermal Science and Engineering Progress 23 (2021) 100920, https://doi.org/10.1016/j.tsep.2021.100920.
[29] B. Xu, Z. Li, Paraffin/diatomite/multi-wall carbon nanotubes composite phase change material tailor-made for thermal energy storage cement-based composites, Energy 72 (2014) 371–380, https://doi.org/10.1016/j.energy.2014.05.049.
[30] Z. Zhang, G. Shi, S. Wang, X. Fang, X. Liu, Thermal energy storage cement mortar containing n-octadecane/expanded graphite composite phase change material, Renew. Energy 50 (2013) 670–675, https://doi.org/10.1016/j.renene.2012.08.024.
[31] K.S. Kim, Y. Zhao, H. Jang, S.Y. Lee, J.M. Kim, K.S. Kim, J.-H. Ahn, P. Kim, J.-Y. Choi, B.H. Hong, Large-scale pattern growth of graphene films for stretchable transparent electrodes, Nature 457 (2009) 706–710, https://doi.org/10.1038/nature07719.
[32] M.D. Stoller, S. Park, Y. Zhu, J. An, R.S. Ruoff, Graphene-based ultracapacitors, Nano Letters 8 (2008) 3498–3502, https://doi.org/10.1021/nl802558y.
[33] C. Lee, X. Wei, J.W. Kysar, J. Hone, et al., Measurement of the elastic properties and intrinsic strength of monolayer graphene, Science 321 (2008) 385–388, https://doi.org/10.1126/science.1157996.
[34] A.A. Balandin, S. Ghosh, W. Bao, I. Calizo, D. Teweldebrhan, F. Miao, C.N. Lau, Superior thermal conductivity of single-layer graphene, Nano Lett. 8 (2008) 902–907, https://doi.org/10.1021/nl0731872.
[35] D.W. Johnson, B.P. Dobson, K.S. Coleman, A manufacturing perspective on graphene dispersions, Current Opinion in Colloid and Interface Science 20 (2015) 367–382, https://doi.org/10.1016/j.cocis.2015.11.004.
[36] https://www.rubitherm.eu/media/products/datasheets/Techdata_-RT24_EN_09102020.PDF, Accessed 20th October 2023.
[37] https://www.microteklabs.com/product-data/nextek-24d/, Accessed 20th October 2023.
[38] https://puretemp.com/wp-content/uploads/2021/06/PureTemp25TechnicalDataSheet.pdf, Accessed 20th October 2023.
[39] A. Zurutuza-Elorza, B. Alonso-Rodriguez, Method for obtaining graphene oxide, in: European Patent, No. 3,070,053B1. European Patent Office, 2015.
[40] S.E. Gustafsson, Transient plane source techniques for thermal conductivity and thermal diffusivity measurements of solid materials, Rev. Sci. Instrum. 62 (1991) 797–804, https://doi.org/10.1063/1.1142087.
[41] T. Log, S.E. Gustafsson, Transient plane source (TPS) technique for measuring thermal transport properties of building materials, Fire and Materials 19 (1) (1995) 43–49, https://doi.org/10.1002/fam.810190107.
[42] DIN EN ISO 22007-2:2021-05, Plastics- Determination of Thermal Conductivity and Thermal Diffusivity- Part 2: Transient Plane Heat Source (Hot Disc) Method, ISO/DIS 22007–2, 2021.
[43] E.W. Washburn, The dynamics of capillary flow, Phys. Rev. 17 (3) (1921) 273–283, https://doi.org/10.1103/PhysRev.17.273.
[44] D. Snoeck, B. Priem, P. Dubruel, N. de Belie, Encapsulated phase-change materials as additives in cementitious materials to promote thermal comfort in concrete constructions, Mater. Struct. 49 (2016) 225–239, https://doi.org/10.1617/s11527-014-0490-5.
[45] M. Sam, A. Caggiano, L. Dubyey, J.-L. Dauvergne, E. Koenders, Thermo-physical and mechanical investigation of cementitious composites enhanced with microencapsulated phase change materials for thermal energy storage, Construct. Build Mater. 340 (2022) 127585, https://doi.org/10.1016/j.conbuildmat.2022.127585.
[46] Y. Wang, Q. Li, W. Miao, Y. Su, X. He, B. Strnadel, The thermal performances of cement-based materials with different types of microencapsulated phase change materials, Construct. Build Mater. 345 (2022) 128388, https://doi.org/10.1016/j.conbuildmat.2022.128388.
[47] B. Zalba, J.M. Marín, L.F. Cabeza, H. Mehling, Review on thermal energy storage with phase change: materials, heat transfer analysis and applications, Appl. Therm. Eng. 23 (2003) 251–283, https://doi.org/10.1016/S1359-4311(02)00192-8.
[48] Y. Zeng, T. Li, Y. Yao, T. Li, L. Hu, A. Marconnet, Thermally conductive reduced graphene oxide thin films for extreme temperature sensors, Adv. Funct. Mater. 29 (2019) 1901388, https://doi.org/10.1002/adfm.201901388.
[49] J.D. Renteria, S. Ramirez, H. Malekpour, B. Alonso, A. Centeno, A. Zurutuza, A. I. Cocemasov, D.L. Nika, A.A. Balandin, Strongly anisotropic thermal conductivity of free-standing reduced graphene oxide films annealed at high temperature, Adv. Funct. Mater. 25 (2015) 4664–4672, https://doi.org/10.1002/adfm.201501429.
[50] K.-H. Kim, S.E. Jeon, J.K. Kim, S. Yang, An experimental study on thermal conductivity of concrete, Cem. Concr. Res. 33 (2003) 363–371, https://doi.org/10.1016/S0008-8846(02)00965-1.
[51] G. Goracci, J.S. Dolado, Elucidation of conduction mechanism in graphene nanoplatelets (GNPs)/cement composite using dielectric spectroscopy, Materials 13 (2) (2020) 275, https://doi.org/10.3390/ma13020275.
[52] G. Goracci, D.M. Salgado, J.J. Gaitero, J.S. Dolado, Electrical conductive properties of 3D-printed concrete composite with carbon nanofibers, Nanomaterials 11 (2022) 3939, https://doi.org/10.3390/nano12223939.
[53] E. Erkizia, C. Strunz, J.-L. Dauvergne, G. Goracci, I. Peralta, A. Serrano, A. Ortega, B. Alonso, F. Zanoni, M. Düngfelder, J.S. Dolado, J.J. Gaitero, C. Mankel, E. Koenders, Cement based materials with PCM and reduced graphene oxide for thermal insulation for buildings, in: A. Jędrzejewska, F. Kanavaris, M. Azenha, F. Benboudjema, D. Schlicke (Eds.), International RILEM Conference on Synergising Expertise towards Sustainability and Robustness of Cement-Based Materials and Concrete Structures. SynerCrete 2023. RILEM Bookseries vol. 43, Springer, Cham, 2023, pp. 1–13, https://doi.org/10.1007/978-3-031-33211-1_113.
[54] T.J. Riazzi, A non-flammable coating loaded with microcapsules encapsulating a flammable phase change material and layered structures made therewith, International application number PCT/US2021/038379, in: International Publication Number WO 2021/262653 A1, filing date: 22/06/2021, 30/12/2021 publication date, https://patentimages.storage.googleapis.com/62/97/51/99de93abdbc81c/WO2021262653A1.pdf.
[55] Standards that apply: ISO 11357, ASTM E967, ASTM E968, ASTM E793, ASTM D3895, ASTM D3417, ASTM, D3418, DIN 51004, DIN 51007 and DIN 53765.
[56] S. Diamond, Physical and Chemical Characteristics of Cement Composites in Durability of Concrete and Cement Composites, Woodhead Publishing, 2007.
[57] M.J. McCarthy, T.D. Dyer, "Pozzolanas and Pozzolanic Materials," in Lea's Chemistry of Cement and Concrete, Fifth edition, Butterworth-Heinemann, 2019.
[58] J. Texter, Graphene dispersions, Current Opinion in Colloid and Interface Science 19 (2014) 163–174, https://doi.org/10.1016/j.cocis.2014.04.004.
[59] S.W. Sharshir, A. Joseph, M. Elsharkawy, M.A. Hamada, A.W. Kandeal, M. R. Elkadeem, A.K. Thakur, Y. Ma, M.E. Moustapha, M. Rashad, M. Arici, Thermal energy storage using phase change materials in building applications: a review of recent development, Energy & Buildings 285 (2023) 112908, https://doi.org/10.1016/j.enbuild.2023.112908.
[60] X. Liu, Z. Rao, Experimental study on the thermal performance of graphene and exfoliated graphite sheet for thermal energy storage phase change material, Thermochim. Acta 647 (2017) 15–21, https://doi.org/10.1016/j.tca.2016.11.010.
[61] R.J. Warzoha, A.S. Fleisher, Improved heat recovery from paraffin-based phase change materials due to the presence of percolating graphene networks, Int. J. Heat Mass Transf. 79 (2014) 314–323, https://doi.org/10.1016/j.ijheatmasstransfer.2014.08.009.